第 33 卷 第 1 期　　焊　接　学　报　　Vol. 33　No. 1
2012 年 1 月　　TRANSACTIONS OF THE CHINA WELDING INSTITUTION　　January　2012

TiAl 合金与镍基高温合金的扩散连接

何　鹏[1]，李海新[1]，林铁松[1]，黄玉东[2]，刘　羽[1]，钱国统[3]

(1. 哈尔滨工业大学 先进焊接与连接国家重点实验室，哈尔滨　150001；
2. 哈尔滨工业大学 化工学院，哈尔滨　150001；
3. 绍兴市天龙锡材有限公司，绍兴　312001)

何　鹏

摘　要：采用钛为中间层，对 TiAl 合金与镍基高温合金(GH99)进了扩散连接. 研究了扩散连接接头的界面结构和连接温度对界面结构及连接性能的影响，并对连接界面反应层的形成机制进行探讨. 结果表明，GH99/Ti/TiAl 的界面结构为：GH99/$(Ni,Cr)_{ss}$/富 Ti-$(Ni,Cr)_{ss}$/TiNi/Ti_2Ni/α-Ti + Ti_2Ni/$Ti(Al)_{ss}$/TiAl + Ti_3Al/TiAl；随着连接温度的升高，各反应层厚度增加，接头的抗剪强度先增加后减小；在连接温度 1 173 K，连接时间 30 min，连接压力 20 MPa 时，抗剪强度最高为 260.7 MPa.

关键词：钛铝合金；镍基高温合金；扩散连接；界面结构
中图分类号：TG457　　**文献标识码**：A　　**文章编号**：0253－360X(2012)01－0017－04

0　序　　言

TiAl 合金是应用于航空、航天飞行器热端部件的理想候选材料[1]，相比于传统应用的镍基高温合金，TiAl 合金的部分取代能显著减轻飞行器的重量，提高其发射及飞行效率. 因此研究 TiAl 合金与镍基高温合金的连接对于加强 TiAl 合金在航空航天等领域的广泛应用具有重要意义. 目前，用于 TiAl 合金连接的方法主要有氩弧焊、电子束焊、摩擦焊、钎焊和扩散焊等[2-6]，其中扩散连接可以实现异种材料高精度、高质量的连接，且可控制焊缝中脆性金属间化合物的生成. 因此，大多数情况下采用扩散连接方法实现 TiAl 合金与异种材料的连接[7].

TiAl 合金与 Ni 基高温合金直接扩散连接时，大量 Ti-Ni-Al 三元金属间化合物的生成导致强度较低[8]. Li 和 Luo 等人[1,3]用超塑性扩散连接能够在比常规扩散连接低的温度下，得到比直接扩散连接强度高的接头. Ramos 等人[9]采用多层纳米 Ni/Al 薄层作为中间层也实现了 γ-TiAl 合金与镍基合金的连接. 但超塑性扩散连接和磁控溅射镀膜作中间层的扩散连接，工艺复杂，成本较高，对于实际应用中的一些大型复杂构件，难以操作.

文中采用钛箔作中间层扩散连接 TiAl 及镍基高温合金，克服采用超塑性扩散连接和磁控溅射中间层扩散连接等方法成本高、对母材表面状态要求高及工艺复杂的缺点，对焊后接头的界面结构和性能进行系统研究，揭示了界面反应层的形成机制.

1　试验方法

试验材料用 TiAl 合金与镍基高温合金(型号为 GH99)，化学成分见表 1. 中间层采用纯钛箔，厚度为 80 μm. 用电火花线切割将 TiAl 合金加工成 7 mm × 5 mm × 2 mm，将 GH99 合金分别加工成 7 mm × 5 mm × 1.2 mm 的界面组织观察试样和 14 mm × 5 mm × 1.2 mm 的强度测试试样，将待焊试样表面用金相砂纸逐级磨光，随后将磨好的 TiAl 和 GH99 母材及钛箔在丙酮中超声清洗 10 min，按图 1 装配，在真空辐射加热的多功能前置炉(真空度为 2.3×10^{-5} MPa)中进行扩散连接. 采用扫描电镜、电子探针和 X 射线衍射等方法分析连接界面，焊后依据标

表 1　试验材料化学成分(摩尔分数，%)
Table 1　Chemical compositions of materials

	Al	Ni	Cr	Ti	V	Co	W	Mo	Si
TiAl	52.8	—	1.2	44.9	1.1	—	—	—	—
GH99	5.4	57.3	20.6	2.0	0.4	7.5	3.0	3.0	0.8

收稿日期：2010－10－12
基金项目：国家自然科学基金资助项目(50975062，51105107，51021002)；黑龙江省自然科学基金资助项目(QC2011C044)；中国国家博士后基金资助项目(AUGA4130902510)；中央高校基本科研业务费专项资金资助项目(HIT. BRETI. 2010006，HIT. NSRIF. 2010119，HIT. NSRIF. 201135)

准 DIN 8526—1977，以抗剪强度值评价接头连接强度. 剪切试验在 INSTRON MODEL1186 电子万能试验机上进行，加载速度为 1 mm/min.

2 试验结果及分析

2.1 界面结构

图 2 为连接温度 1 173 K，连接时间 30 min，连接压力 20 MPa 时，GH99/Ti/TiAl 接头的背散射电子像. 可以看出，GH99/Ti 和 Ti/TiAl 的连接界面结合良好. 对两侧界面及钛中间层进行放大，由图 2b 可知，GH99/Ti 界面处存在四层连续反应层，靠近 GH99 侧有两层弥散分布白色相的反应层 *A* 和 *B*，其中，A 层的白色相呈长条状，B 层的白色相呈颗粒状；靠近钛侧为灰白色反应层 D，在 B 和 D 之间为浅灰色反应层 C；Ti/TiAl 连接界面处存在一层灰色反应层 F，在 F 和 TiAl 之间存在一层厚度仅为 1 μm 左右的灰白色颗粒组成的反应层 *G*（图 1d）；中间层钛转变为灰色基体上弥散分布有白色蠕虫状组织的 E 反应层（图 2c）.

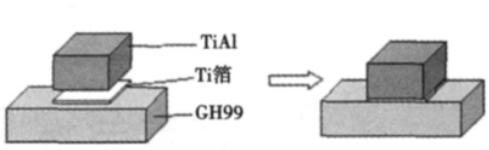

图 1 扩散焊接头示意图

Fig. 1 Schematic of assembling joint

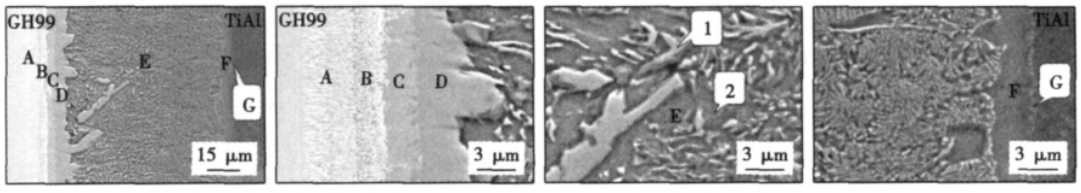

(a) 界面组织全貌 (b) GH99/Ti界面反应层 (c) Ti中间层反应形貌 (d) Ti/TiAl界面反应层

图 2 GH99/Ti/TiAl 界面形貌

Fig. 2 Interfacial microstructure of GH99/Ti/TiAl

图 3 为接头断口的 X 射线衍射结果，可知接头中有 TiNi，Ti_2Ni 和 $(Ti)_{ss}$（ss 表示固溶体）生成，W 为 GH99 中的强化元素，说明连接接头主要断裂于 GH99/Ti 界面处. 界面反应层能谱分析结果如表 2 所示. 由图 3 及表 2 可知，A 层为 $(Ni,Cr)_{ss}$，且含有少量 Ti，Al 元素及来自于 GH99 中的强化元素 W，Mo 和 Co；反应层 B 也为 $(Ni,Cr)_{ss}$，但由于距离 Ti 中间层较近，Ti 含量较高，称其为富 Ti-$(Ni,Cr)_{ss}$；反应层 C 和 D 分别为 TiNi 和 Ti_2Ni；反应层 E 中的白色蠕虫状组织 1 为 Ti_2Ni，灰色基底 2 为 α-Ti，因此，E 层为灰色 α-Ti 基体上弥散分布 Ti_2Ni 相的反应层；反应层 F 为 $Ti(Al)_{ss}$；由于反应层 G 组织非常细小，能谱测试时会受到周围组织成分的影响，但根据结果推断其为 $TiAl + Ti_3Al$. 综上，GH99/Ti/TiAl 接头的界面结构为：GH99/$(Ni,Cr)_{ss}$/富 Ti-$(Ni,Cr)_{ss}$/TiNi/Ti_2Ni/α-Ti + Ti_2Ni/Ti $(Al)_{ss}$/TiAl + Ti_3Al/TiAl.

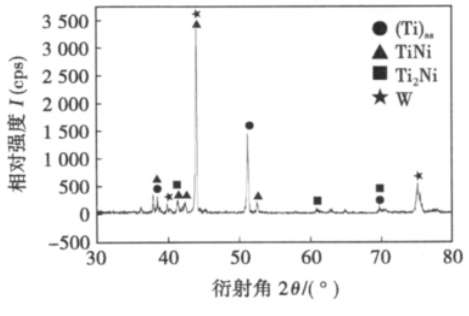

图 3 接头断口的 X 射线衍射分析

Fig. 3 XRD pattern of fracture in joint

表 2 连接接头各反应层元素含量（摩尔分数，%）

Table 2 Chemical composition of reaction layers

反应层	Al	W	Mo	Co	Ti	Cr	Ni	可能相
A	5.2	4.0	4.1	7.1	6.8	23.5	49.5	$(Ni,Cr)_{ss}$
B	8.5	4.7	4.5	6.9	20.7	28.9	25.8	富 Ti-$(Ni,Cr)_{ss}$
C	0.7	0.3	0.7	8.2	47.5	2.3	40.3	TiNi
D	0.9	0.7	0.6	2.8	62.9	0.8	31.2	Ti_2Ni
E1	1.8	0.3	0.3	0.7	66.6	1.0	30.4	Ti_2Ni
E2	5.2	0.5	0.5	0.9	91.1	0.8	1.0	α-Ti
F	16.0	0.6	0.5	0.7	81.2	0.5	0.7	$Ti(Al)_{ss}$
G	35.0	0.2	0.4	0.5	57.2	1.5	5.1	$TiAl + Ti_3Al$

2.2 连接温度对界面结构及连接强度的影响

连接温度是扩散连接中最重要的参数，温度越高，材料的塑性越好，元素的活性越大，则可以在较

小的压力和较短的时间内实现连接.

图 4 为连接时间 30 min,连接压力 20 MPa 时,不同连接温度下的界面组织结构. 由图 4a 可以看出,当连接温度为 1 073 K 时,Ti/TiAl 界面处存在未焊合孔洞,这是由于温度较低,原子扩散不充分造成的. 当温度为 1 123 K 时,两侧界面结合较好,且在中间层钛中开始生成大量的 Ti_2Ni 相,但分布不均匀(图 4b). 随着连接温度继续升高,界面处原子扩散相对增加,界面反应进行得更加充分,Ti_2Ni 在钛上均匀分布,且各反应层厚度显著增加(图 4c).

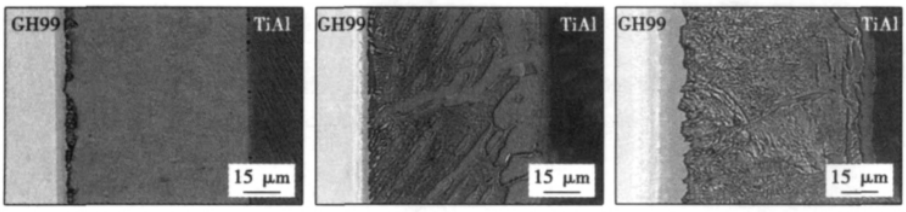

(a) 1 073 K　(b) 1 123 K　(c) 1 193 K

图 4　不同温度下的 GH99/Ti/TiAl 界面形貌

Fig. 4　Interfacial microstructure of GH99/Ti/TiAl at different temperatures

图 5 为不同连接温度下扩散连接接头的室温抗剪强度. 由图 5 中看出,抗剪强度值随温度先升高后降低. 温度较低时(1 073 K),界面结合处反应不充分,存在少量未焊合孔洞(图 4a),影响连接强度;当温度继续升高到 1 173 K 时,界面反应充分,无缺陷,GH99 界面处各反应层厚度大致相当(图 2a),有利于提高接头强度. 因此,在连接温度1 173 K,连接时间 30 min,连接压力 20 MPa 时,接头的抗剪强度最高,达到 260.7 MPa. 但当温度继续升高时,各反应层厚度增加(图 4c),焊缝中残余应力较大,导致接头强度降低.

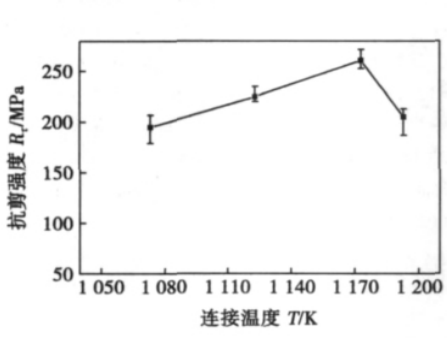

图 5　连接温度对接头抗剪强度的影响

Fig. 5　Effect of bonding temperature on shear strength of joint

3　界面反应机制

3.1　GH99/Ti 界面反应机制

GH99/Ti 界面结构的形成大致分为四个阶段: I. GH99 中的 Ni 原子向钛箔中扩散,同时钛箔中 Ti 原子向 GH99 中扩散,根据 Ti-Ni 二元合金相图,镍在钛中的扩散速度大于钛在镍中的扩散速度,当镍在钛中的浓度达到 4.5%(摩尔分数)时,就会发生如式(1)的共析反应,Ti_2Ni 反应层生成(图 6b);II. 随着镍向钛中扩散量增加,在 GH99 界面处含镍量降低,同时合金元素浓度增加,即合金元素偏聚区 $(Ni,Cr)_{ss}$ 形成(图 6c);III. 在浓度梯度作用下,Ni 原子继续向钛箔侧扩散,使得界面处镍浓度增加,当增加到一定程度,按照式(2),生成 TiNi 反应层(图 6d);Ⅳ. 随着镍的进一步扩散,导致与 TiNi 紧邻的 $(Ni,Cr)_{ss}$ 的界面处镍浓度降低,另外 Ti 原子会继续向 GH99 侧扩散,因此,在此界面处,镍浓度降低,钛浓度升高,导致富 Ti-$(Ni,Cr)_{ss}$ 反应层生成(图 6e).

$$\beta Ti \leftrightarrow \alpha Ti + Ti_2Ni \quad (1)$$

$$Ti_2Ni + Ni \rightarrow TiNi \quad (2)$$

3.2　Ti/TiAl 界面反应机制

Ti/TiAl 界面结构的形成可大致分为两个阶段:在一定的连接条件下,当钛箔与 TiAl 紧密接触时,在浓度梯度的作用下,原子之间发生互扩散,即 TiAl 中的 Al 原子与钛箔中的钛原子相互扩散. 由于铝的原子半径较小,其在 Ti 中的扩散速度要比 Ti 在 TiAl 中的扩散速度快,因此铝由 TiAl 侧向钛中扩散,按照式(3),首先在 Ti/TiAl 界面处生成 $Ti(Al)_{ss}$ 反应层(图 7b). 然后,在浓度梯度作用下,钛箔中的 Ti 原子向 TiAl 中扩散,使得界面处 Ti 原子浓度逐渐增加,当浓度增加到一定程度时,按照式(4),界面处形成 $Ti_3Al + TiAl$ 反应层(图 7c)[10].

$$Ti + Al \rightarrow Ti(Al)_{ss} \quad (3)$$

$$TiAl + Ti \rightarrow Ti_3Al \quad (4)$$

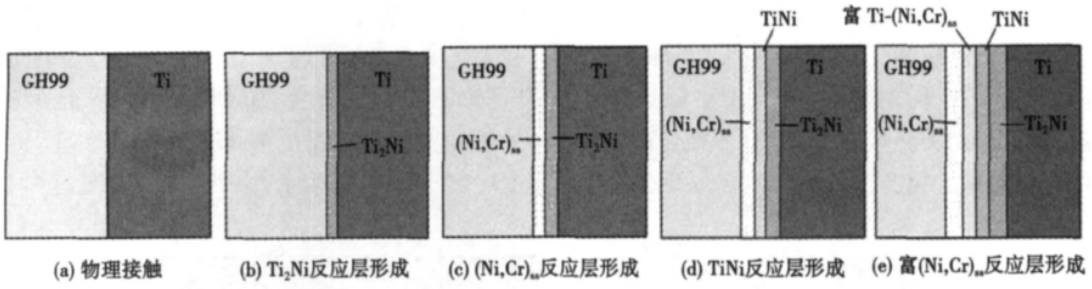

图 6 GH99/Ti 界面组织转变示意图

Fig. 6 Schematic showing interface reaction of GH99/Ti

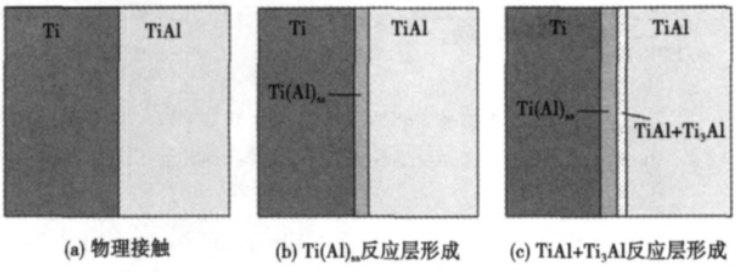

图 7 Ti/TiAl 界面组织转变示意图

Fig. 7 Schematic diagram of interface reaction of Ti/TiAl

4 结 论

(1) 用钛中间层可以成功实现 TiAl 与 GH99 合金的扩散连接，所得界面结构为: GH99/$(Ni,Cr)_{ss}$/富 Ti-$(Ni,Cr)_{ss}$/TiNi/Ti_2Ni/α-Ti + Ti_2Ni/Ti(Alss)/TiAl + Ti_3Al/TiAl.

(2) 随着连接温度升高，接头抗剪强度先增加后减小，当连接温度 1 173 K，连接时间 30 min，连接压力 20 MPa 时，抗剪强度最高为 260.7 MPa.

(3) 分析界面反应层的形成机制，得出 GH99/Ti 界面处反应层的形成顺序依次为: Ti_2Ni，$(Ni,Cr)_{ss}$，TiNi 和富 Ti-$(Ni,Cr)_{ss}$; Ti/TiAl 界面处 $Ti(Al)_{ss}$ 反应层首先形成，随着元素进一步扩散，TiAl + Ti_3Al 反应层形成.

参考文献:

[1] Luo G X, Wu G Q, Huang Z, *et al*. Diffusion bonding of laser-surface-modified gamma titanium aluminide alloy to nickel-base casting alloy [J]. Scripta Materialia. 2007, 57: 521 - 524.

[2] Mallory L C. Microstructure of titanium aluminide fusion welding [J]. Journal of Materirals Science Letter, 1994, 13: 1061 - 1065.

[3] Wu H Q, Feng J C, He J S, *et al*. Microstructural characterization of electron beam welded joints of TiAl-based intermetallic compound [J]. Rare Metals, 2005, 24(1): 82 - 86.

[4] 宫下卓也，日野春树. TiAl 金属间化合物の摩擦压接特性 [J]. 日本金属学会志，1994，58(2)：215 - 220.

[5] Lee S J, Wu S K, Lin R Y. Infrared joining of TiAl intermetallics using Ti-15Cu-15Ni foil-Ⅰ. The microstucture morphologies of joint interfaces [J]. Acta Materialia, 1998, 46(4): 1283 - 1295.

[6] Wang X F, Ma M, Liu X B. Diffusion bonding of γ-TiAl alloy to Ti-6Al-4V alloy under hot pressure [J]. Transactions of Nonferrous Metals Society of China, 2006, 16(5): 1059 - 1063.

[7] 何 鹏，冯吉才，韩杰才，等. TiAl 金属间化合物及其连接技术的研究进展 [J]. 焊接学报，2002，23(5)：91 - 95.
He Peng, Feng Jicai, Han Jiecai, *et al*. Advances in TiAl intermetallics and its joining technology (Ⅱ)—Advances in TiAl intermetallics [J]. Transactions of the China Welding Institution, 2002, 23(5): 91 - 95.

[8] Li Z F, Wu G Q, Huang Z, *et al*. Diffusion bonding of laser surface modified TiAl alloy/Ni alloy [J]. Materials Letters, 2004, 58: 3470 - 3473.

[9] Ramos A S, Vieiral M T, Simões, *et al*. Joining of superalloys to intermetallics using nanolayers [J]. Advanced Materials Research, 2009, 59: 225 - 229.

[10] He P, Feng J C, Zhang B G, *et al*. A new technology for diffusion bonding intermetallic TiAl to steel with composite barrier layers [J]. Materials characterization, 2003, 50: 87 - 92.

作者简介： 何 鹏，男，1972 年出生，博士研究生导师，教授. 主要从事新材料及异种材料的研究工作. 已发表论文 100 余篇.
Email: hithepeng@hit.edu.cn

通讯作者： 林铁松，男，讲师. Email: tiesonglin@hit.edu.cn

MAIN TOPICS, ABSTRACTS & KEY WORDS

Design and implementation of a power control system for electron beam welder HE Shaojia, LI Jianling, MO Jinhai, LI Haibiao (School of Mechanical & Electrical Engineering, Guilin University of Electronic Technology, Guilin 541004, China). pp 1 – 5, 12

Abstract: Stability of output voltage of high-voltage accelerating stabilized power supply for electron beam welder (EBW) is a prerequisite to ensure the electron beam welding quality. The common power supplies have the disadvantages of circuit complexity and bulkiness. A novel control system of high-voltage accelerating stabilized power supply for EBW was designed. Its main circuit is based on pulse-width modulation (PWM) buck-boost converter topology. Compared with common EBW power supplies, this new power supply requires a much lower voltage grade transformer because of the converter's effect for rising voltage, so its volume is smaller and the circuit is simpler. The system main circuit characteristics and its working process were analyzed. The system circuit's small-signal mathematical model was created, and lag-lead correction compensation control was employed in the system to achieve static and dynamic performance requirements. The results displayed that this unit had the characteristics of fast response, high reliability, high control precision and anti-interference capability.

Key words: electron beam welder; buck-boost converter; simulation

Effects of ultrasonic on properties of joints welded by friction stir welding process MA Huikun, HE Diqiu, LIU Jinshu (College of Mechanical and Electrical Engineering, Central South University, Changsha 410083, China). pp 6 – 8

Abstract: In this paper, joints of 2219, 7A52 and LF21 aluminum alloy were obtained by using a self-made ultrasonic friction stir welding machine. The microstructures and fractography of these joints were studied. The results show that the thermal mechanically affected zone (TMAZ) of ultrasonic friction stir welding is almost disappearing; The grains of weld nugget zone (WNZ) by ultrasonic friction stir welding are much finer than the ones obtained by conventional friction stir welding; The tensile fracture of base material appears to be mixed fracture with dimple and tear ridges. The tensile fracture of ultrasonic friction stir welding appears to be a dimple pattern. Although the tensile strength of joints obtained by ultrasonic friction stir welding are higher than the ones obtained by conventional friction stir welding, the elongation of the joints fellow on opposite tendency.

Key words: friction stir welding; ultrasonic; property

Effects of welding materials on hot crack of spray formed 7475 Aluminum alloy in TIG welding joint YAN Keng, YE Youli, WANG Xiling (Provincial Key Lab of Advanced Welding Technology, Jiangsu University of Science and Technology, Zhenjiang 212003, China). pp 9 – 12

Abstract: In this paper, the spry formed 7475 aluminium alloy was welded by TIG welding process with the welding consumable 4043, 5356 and 7055 respectively. The susceptibilities of hot cracking, as well as the mechanical properties, microstructures, the morphologies and the phase compositions of joints were studied in all three kinds of welding consumables. The results showed that susceptibility of hot cracking of welding material 5356 was closely related to the heat input. In condition of high heat input, Cu and Zn in parental material diffuse to weld and form low melting point eutectic phased α-Al, $Al_{0.403}Zn_{0.597}$ and $Al_7Cu_3Mg_6$ at fusion area with Mg from weld. And then they segregate at inter-granular and inter-dendrite. Therefore, penetrated hot cracks appeared in the fusion area under the action of welding stress. No crack appeared in condition of low heat input but the tensile strength of welded joint was only 184MPa. However, hot cracking susceptibilities of welding consumables 4043 and 7055 are relatively lower.

Key words: spray formed aluminum alloy; TIG welding; hot crack

A analysis method of seam tracking accuracy based on wheeled robot HONG Bo, ZHANG Qilin, LI Xiangwen, YIN Li (School of Mechanical Engineering, Xiangtan University, Xiangtan 411105, China). pp 13 – 16

Abstract: Based on the research of the wheeled robot seam tracking accuracy in 4 degrees of freedom, a new characterization assessment of seam tracking accuracy method was proposed, and 5-parameter model under D-H coordinate system in seam bias was built up as well. By this model, the main error sources affecting the accuracy of seam tracking is theoretically analyzed. Through the simulation analysis of fixed-step and variable step method of seam tracking control, the correctness and validity to accuracy of analytical methods and modeling presented in this paper were verified, the main reason affecting seam tracking accuracy was seam tracking control algorithm and robot positioning accuracy. The accuracy analysis method have guiding significance for seam tracking control of robot error compensation and the improvement of seam tracking control method.

Key words: seam tracking; robot; accuracy analysis

Diffusion bonding of TiAl to Ni-based superalloy HE Peng[1], LI Haixin[1], LIN Tiesong[1], Huang Yudong[2], LIU Yu[1], QIAN Guotong[3] (1. State Key Laboratory of Advanced Welding and Joining, Harbin institute of Technology, Harbin 150001, China; 2. School of Chemical Engineering and Technonlgy, Harbin institute of Technology, Harbin 150001, China; 3. Shaoxing Tianlong Tin Materials CO., LTD, Shaoxing 312001, China).

pp 17 – 20

Abstract: Diffusion bonding of TiAl to Ni-based alloy using Ti interlayer was studied. The microstructure of the joint and effect of bonding temperature on microstructure and properties of the joint were investigated, and the mechanism of the formation of reaction layers was also discussed. The experiment results show that the interfacial structure of the GH99/Ti/TiAl joint is GH99/(Ni,Cr)$_{ss}$/rich Ti-(Ni,Cr)$_{ss}$/TiNi/Ti_2Ni/α-Ti + Ti_2Ni/Ti(Al)$_{ss}$/TiAl + Ti_3Al/TiAl. With the bonding temperature increasing, the thickness of reaction layers increases. The shear strength of the joint increases with the bonding temperature, and goes through a maximum at 1173 K/30 min/20 MPa and thereafter falls off. The maximum shear strength is 260.7 MPa.

Key words: titanium aluminium alloy; Ni-based superalloy; diffusion bonding; interfacial structure

Microstructure and properties of radial friction welded joint of 37CrMnMo steel pipe QIN Guoliang[1], ZHANG Chunbo[2], ZHOU Jun[2], QI Xiubin[2], ZHANG Yan[2] (1. Institute of Advanced Welding Technology, Shandong University, Jinan 250061, China; 2. Harbin Welding Institute, Harbin 150080, China). pp 21 – 24

Abstract: With self-developed radial friction welding machine, 37CrMnMo steel pipe was welded at the optimized welding parameters by taking 45 steel as ring. Experimental results show that the ring has serious plastic deformation and there is a narrow HAZ in 37CrMnMo steel pipe body and the weld is oxidized. The mean shear strength of the weld can be up to 401 MPa, which is higher than that of 45 steel. The appearance of shear fracture is smooth and characterized by shear dimple, which indicates that the weld has high ductile and plastic properties. The microhardness is decreased from the bonding center to both sided of 45 steel ring and 37CrMnMo steel pipe. The analyses on microstructure of the joint show that there is a very good narrow metallurgical bonding zone between steel ring and steel pipe, but overheated zones appears in HAZ of 45 steel pipe and 20 steel ring. The HAZ in 45 steel side is ferrite, pearlite and bainite, and that in 37CrMnMo steel side is bainite and a few martensite. Compared with base metal, hardening microstructure appears in HAZs of 45 steel and 37CrMnMo steel because of high cooling rate, but the microstructure in the weld is finer than that of base metal under the thermo-mechanical coupling interaction.

Key words: radial friction welding; steel pipe welding; joint; microstructure; mechanical properties

Welding currents filtering of compulsively short circuiting transfer in rotational arc MAG welding GAO Yanfeng[1,2], XIAO Jianhua[1], ZHANG Hua[2] (1. School of Aeronautical Manufacturing Engineering, Nanchang Hangkong University, Nanchang 330063, China; 2. School of Mechanical & Electrical Engineering, Nanchang University, Nanchang 330031, China). pp 25 – 28

Abstract: The present paper describes the welding current characteristics of rotational arc MAG welding in V groove. It is found that the compulsively short circuiting transfer would take place when the welding gun rotates to the sides of V groove. The reason for this phenomenon is that the contact tip distance between the wire tip and workpiece becomes short when the welding gun moves to the sides of groove. During the period of short circuiting transfer, the welding currents would sharply increase, so as to affect the rotational arc sensor sensitivity. A hybrid filtering method based on spatial neighborhood mean filter and soft threshold wavelet filter is proposed to process the welding currents, and the real-time characteristics of this method is researched in this paper as well. The experimental results show that the hybrid filtering method has a higher filtering property and better real-time character. This study will set up the foundation for the welding gun deviation identification in the welding seam tracking.

Key words: rotational arc welding; short circuiting transfer; welding currents; wavelet filtering

Laser-arc hybrid welding of T-type structure of titanium sheet LI Chenbin, LIU Liming (Key Laboratory of Liaoning Advanced Welding and Joining Technology, Dalian University of Technology, Dalian 116024, China). pp 29 – 32

Abstract: Low powered laser-arc hybrid welding was used to weld T-type structure of titanium sheet. The welding joints were investigated via the optical microscopy, X-ray diffractometer. Results showed that laser could induce arc and enhance the penetrability of arc in laser-arc hybrid welding process and welding of T-type structure of titanium sheet was easily achieved. The close ripples form on the top surface of the welding seam, and the welding joint is full-penetration and gentile on the back. The welding seam is made up of α′-phase and β-phase. The acicular α′ is loose and disheveled because of the stirring effect of pulsed laser, pulsed TIG, spray of metal vapor and plasma. The contents of Al and Mn are maintained steadily, and there is no component segregation.

Key words: T-type structure; hybrid welding; titanium alloy

Control method for nugget size of resistance spot welding of three-layer steels with different thickness and strength SHEN Jie, LIN Haolei, ZHANG Yansong, CHEN Guanlong (Shanghai Key Laboratory of Digital Autobody Engineering, Shanghai Jiaotong University, Shanghai 200240, China). pp 33 – 36

Abstract: In order to study the nugget formation during resistance spot welding procers of three-layer steels with different strength and thickness, asymmetric electrodes were utilized to improve the nugget size and weldability. Finite element analysis was used to investigate the current density, temperature change and nugget sizes of the thinner side. Experiments were also carried out to analyze nuggets sizes at different welding time. The welding lobes under symmetric and asymmetric electrodes were established. The results showed that the current density and temperature field of the thinner side could be changed significantly as asymmetric electrodes were applied, which could facilitate the formation of nugget and widen the weldability of three-layer